Production of Multioriented Polarization for Relativistic Electron Beams via a Mutable Filter for Nonlinear Compton Scattering

Qianyi Ma,[1] Yuhui Tang,[1] Jinqing Yu,[2] Yinren Shou,[1] Xuezhi Wu,[1] and Xueqing Yan[1,3,4,5,*]

[1] *State Key Laboratory of Nuclear Physics and Technology, and Key Laboratory of HEDP of the Ministry of Education, CAPT, School of Physics, Peking University, Beijing 100871, China*

[2] *School of Physics and Electronics, Hunan University, Changsha 410082, China*

[3] *Beijing Laser Acceleration Innovation Center, Huairou, Beijing 101400, China*

[4] *CICEO, Shanxi University, Taiyuan, Shanxi 030006, China*

[5] *Institute of Guangdong Laser Plasma Technology, Baiyun, Guangzhou 510540, China*

(Received 7 February 2022; revised 26 November 2022; accepted 12 December 2022; published 20 January 2023)

We propose a feasible scenario for directly polarizing a relativistic electron beam and obtain an overall polarization in various directions through a filter mechanism for single-shot collisions between an ultrarelativistic unpolarized electron beam and an ultraintense circularly polarized laser pulse. The electrons are scattered over a large angular range of several degrees, and the polarization states of the electrons are connected with their spatial positions after the collision. Therefore, we can employ a filter to filter out a part of the scattered electrons based on their position, and obtain a high degree of overall polarization for the filtered beam. Through Monte Carlo simulations with consideration of spin, polarizations with a degree of up to 62% in arbitrary transverse directions and a longitudinal polarization of up to 10% are obtained for filtered beams with currently achievable laser intensities. We analyze theoretically the formation of the distribution of the scattered electrons and investigate the influence of different initial parameters through simulations to demonstrate the robustness of our scheme. This scenario provides a simple and flexible way to produce relativistic polarized electron beams with various polarization directions.

DOI: 10.1103/PhysRevApplied.19.014058

I. INTRODUCTION

Since the spin properties of relativistic electrons were systematically investigated in the last century [1–7], extensive applications of spin-polarized electron beams have been developed in the fields of high-energy, nuclear, atomic, and particle physics [8,9]. Electrons possessing different polarizations have different cross sections for interacting with other particles. Taking advantage of this, polarized relativistic electron beams have played a crucial role in the measurement of the spin structure of the neutron [10] and nuclei [11], the investigation of parity-nonconservation effects [12–14], the search for physics beyond the standard model [15], and the production of polarized photons [16,17] and highly polarized positrons [16,18] through bremsstrahlung radiation.

At present, two methods are typically utilized to generate relativistic polarized electron beams in experiments. The first is to obtain transversely polarized electron beams directly from a storage ring [9] via the Sokolov-Ternov effect [19,20]. Because it is limited by the field strength, this method takes a rather long time, typically several hours, to acquire a high degree of polarization, oriented in the direction opposite to the magnetic field [21]. If a polarization in another direction is required, e.g., the longitudinal polarizations that are more commonly used in practical applications, an additional spin rotator is required to be inserted into the beamline to alter the direction of polarization [22]. For such ultrarelativistic electron beams with an energy about a few GeV, it is feasible to alter the polarization direction with magnets [23]. The second method uses a multistage approach, where nonrelativistic polarized electrons are first extracted from a polarized photocathode [24,25] or a spin filter [26] and then accelerated to high energy in a linac. The extracted electrons are usually longitudinally polarized, and a Wien filter is a convenient instrument for altering the polarization direction of these low-energy nonrelativistic electrons [27,28]. In addition, measurement of the polarization of relativistic electron beams can be performed by utilizing the mechanisms of Mott scattering [29,30], Møller scattering [31–33], Compton scattering [34,35], and synchrotron radiation [36].

The above traditional methods for producing relativistic polarized electron beams all require the aid of large-scale accelerator facilities, which leads to a high barrier to experimental research that utilizes relativistic polarized electron

*x.yan@pku.edu.cn

beams. With the rapid advancement of ultraintense laser technology in recent years, laser intensities can exceed 10^{23} W/cm^2 [37–39], which makes it possible to produce relativistic polarized electron beams via methods employing ultraintense lasers and get rid of the bulky traditional acceleration devices. Therefore, diverse scenarios have been proposed in theoretical and simulation studies [40]. For instance, when an initially unpolarized ultrarelativistic electron beam collides head-on with an ultraintense elliptically polarized laser pulse, the electron beam is split into two oppositely transversely polarized parts with a splitting angle of approximately tens of milliradians, due to nonlinear Compton scattering [41]. Taking advantage of the asymmetry in the field of a two-color or few-cycle ultraintense laser pulse, an unpolarized ultrarelativistic electron beam can acquire an overall transverse polarization from such a collision with a laser pulse [42–44]. There are also schemes for producing polarized electron beams via hydrogen halide targets prepolarized by ultraviolet photodissociation [45–48] during laser-driven or particle-driven plasma wakefield acceleration [49–51], and a filter can be deployed for wakefield acceleration to increase the polarization degree of the electron beam [52].

In this paper, we propose a filter mechanism that can be used with collisions between an initially unpolarized electron beam and an ultraintense circularly polarized laser pulse to obtain relativistic polarized electron beams with various polarization directions. Through Monte Carlo simulations with consideration of spin, we show that by filtering out a part of the scattered electrons based on their position after the collision, we can easily obtain an overall polarization with a degree of up to 62% in arbitrary transverse directions and a longitudinal polarization of around 10% with currently achievable laser intensities and without any additional spin rotator, as shown in Fig. 1. In this scheme, we employ an ultraintense laser with $a_0 \gg 1$ and an ultrarelativistic electron beam with an energy up to the GeV level, where $a_0 = |e|E_0/m_e\omega_L c$, e is the electron charge, m_e is the rest mass of the electron, c is the speed of light, and E_0 and ω_L are the amplitude and frequency, respectively, of the laser field. To obtain the polarization result that we want, an electron beam with less than 20% energy spread and less than 10-mrad angular divergence is needed to mitigate the impact of the energy spread and angular divergence on the electron spatial distribution. These parameters are similar to those used in the schemes mentioned above employing laser-electron interaction. More details are presented in Secs. II and III. The entire processes of generation, polarization, and utilization of relativistic electron beams can be accomplished within tens of centimeters, which is much less than the distance required for methods based on traditional acceleration devices. Therefore, this method of producing relativistic polarized electron beams may be a better choice for some applications in high-energy physics. For

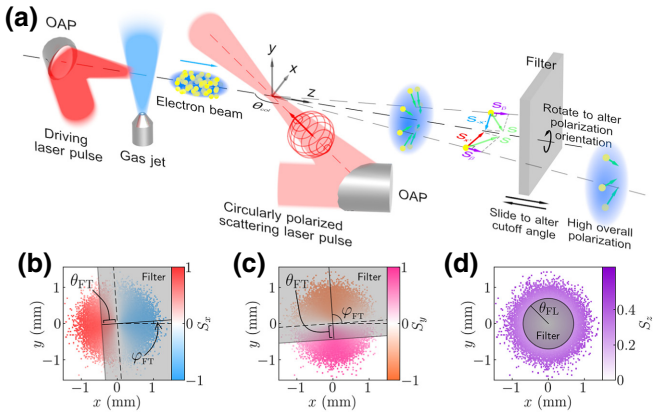

FIG. 1. Scenario for production of relativistic electron beams with multioriented polarization. (a) Schematic layout. (b)–(d) Filter settings to obtain high degrees of polarizations (b) S_x, (c) S_y, and (d) S_z, where the spatial distribution of the electrons is shown at 10 ps after the collision (3 mm behind the collision point). θ_{FT} and φ_{FT} are the cutoff scattering angle and the orientation, respectively, of the filter for transverse polarization. θ_{FL} is the cutoff scattering angle of the filter for longitudinal polarization. OAP is short for the off-axis parabolic mirror.

electrons of several hundred MeV with a broad energy spectrum after nonlinear Compton scattering, traditional spin-rotation systems, using either Wien filters or magnets, cannot be applied to such an electron beam directly, and so a scheme with the ability to produce multioriented polarization shows superiority in those circumstances. Furthermore, we also investigate the results of simulations with different initial parameters and demonstrate the robustness of our scheme.

II. SIMULATION METHODS AND SETUPS

The scenario is illustrated in Fig. 1. A collimated relativistic electron beam propagates along the z axis and collides with an ultraintense circularly polarized laser beam at the origin. The initial electron beam can be extracted from laser-driven plasma wakefield acceleration, where electron beams with energies of up to 8 GeV can be obtained with current state-of-the-art experimental techniques [53,54]. The scattering laser beam, propagating in the horizontal plane (x-z plane), is focused at the origin, and the angle between the laser propagation direction and the electron-beam propagation direction is θ_{col}. Since the filter needs to be placed on the route of the electron beam, a collision angle that does not affect postprocessing of the scattered electrons is chosen rather than a head-on collision.

When electrons interact with an ultraintense laser beam whose normalized laser field a_0 is much greater than 1, nonlinear Compton scattering is dominant in the interaction [55–57]. In the interaction, it is easy to reach the condition for the quantum regime $\chi_e \gtrsim 1$, where $\chi_e =$

$|e|\hbar\sqrt{(F_{\mu\nu}p^{\nu})^2}/m_e^3c^4$ is the invariant quantum efficiency parameter, $\hbar$ is the reduced Planck constant, $F_{\mu\nu}$ is the electromagnetic field tensor, and p^{ν} is the electron four-momentum. The stochastic nature of high-energy photon emission becomes important in the quantum regime, and so a Monte Carlo method is more appropriate for simulations [58,59]. Therefore, to investigate the spin polarization distribution of the scattered electrons, we develop a polarization-vector-based Monte Carlo code [60,61], where both nonlinear Compton scattering and classical spin precession (i.e., the Thomas-Bargmann-Michel-Telegdi (T-BMT) equation [62–64]) are considered.

In our code, the electron spin is described as a three-dimensional normalized polarization vector $\mathbf{S}$ in the rest frame of the electron. The projection of $\mathbf{S}$ indicates the expected value when the polarization is measured along the projection axis. $|\mathbf{S}| = 1$ stands for a fully polarized pure state, $0 < |\mathbf{S}| < 1$ stands for a partially polarized mixed state, and $|\mathbf{S}| = 0$ stands for a completely unpolarized state. In the relativistic theory, we can describe the spin state of an electron in its rest frame using a specially chosen canonical basis $(\boldsymbol{\kappa}, \mathbf{e}, \mathbf{b})$ [61], where $\hat{\mathbf{e}} = \mathbf{E}_{\rm RF}/|\mathbf{E}_{\rm RF}|$ and $\hat{\mathbf{b}} = \mathbf{B}_{\rm RF}/|\mathbf{B}_{\rm RF}|$ are the directions of the electric and magnetic fields, respectively, in the rest frame, and $\hat{\boldsymbol{\kappa}} = \hat{\mathbf{e}} \times \hat{\mathbf{b}}$. When the Lorentz factor $\gamma = 1/\sqrt{1-\boldsymbol{\beta}^2}$, where $\boldsymbol{\beta} = \mathbf{v}/c$ is the velocity of the electron, is much greater than 1, $\hat{\mathbf{e}}$ and $\hat{\mathbf{b}}$ are always orthogonal, and $\hat{\boldsymbol{\kappa}}$ is oriented in the direction opposite to $\boldsymbol{\beta}$.

When $a_0 \gg 1$, the formation interval of the emitted photons becomes very short, proportional to $1/a_0$, and one can neglect the spatiotemporal variation of the background laser field during the process; this is known as the local constant-field approximation (LCFA). We can treat the spin-resolved radiation probability by applying the LCFA. Thus the differential photon emission rate for nonlinear Compton scattering can be derived as [43]

$$\frac{d^2N_\gamma}{d\chi_\gamma\, dt} = \frac{\alpha}{\sqrt{3}\pi\tau_c\gamma\chi_e}\left[\left(2+3\chi_\gamma y\right)K_{2/3}(2y) - \mathrm{Int}\,K(2y) - \frac{\chi_\gamma}{\chi_e}S_b K_{1/3}(2y)\right], \tag{1}$$

where $\tau_c = \hbar/m_e c^2$ is the Compton time, $\alpha = e^2/\hbar c \approx 1/137$ is the fine-structure constant, $y = \chi_\gamma/[3\chi_e(\chi_e - \chi_\gamma)]$, $K_\nu(x)$ is the modified Bessel function of the second kind, $\mathrm{Int}\,K(x) = \int_x^\infty K_{1/3}(z)\,dz$, $S_b = \mathbf{S}\cdot\hat{\mathbf{b}}$, and χ_γ is a quantum parameter related to the photon energy.

In the simulations, the electron particles are moved by the Lorentz force in preset electromagnetic fields and emit photons as follows. First, the instant of emission is decided by the optical depth τ and the final optical depth τ_f assigned to each particle. At the beginning of the simulations, τ is set to 0, and τ_f is sampled from $\tau_f = -\ln\xi_1$, where ξ_1 is a uniform random number in $(0,1)$. The optical depth evolves according to $d\tau/dt = \int_0^{\chi_e}(d^2N_\gamma/d\chi_\gamma\, dt)\,d\chi_\gamma$ [65]. Every time τ reaches τ_f, τ is reset to 0, τ_f is resampled in the same way, and a photon is emitted along $\hat{\boldsymbol{\beta}}$. Next, χ_γ for the photon is decided by use of another uniform random number $\xi_2 \in (0,1]$ from $\xi_2 = [\int_0^{\chi_\gamma}(d^2N_\gamma/d\chi_\gamma\, dt)\,d\chi_\gamma]/[\int_0^{\chi_e}(d^2N_\gamma/d\chi_\gamma\, dt)\,d\chi_\gamma]$. Then, the photon energy can be calculated from $\hbar\omega_\gamma = \gamma m_e c^2\chi_\gamma/\chi_e$. According to momentum conservation, the electron momentum becomes $\mathbf{p}' = \mathbf{p} - (\hbar\omega_\gamma/c)\hat{\mathbf{p}}$ after the emission. In addition, the electron polarization $\mathbf{S}$ is subject to a step alteration after the emission, i.e.,

$$\begin{aligned}\Delta\mathbf{S} = \Bigg\{&\left[\frac{\chi_\gamma}{\chi_e}S_b K_{1/3}(2y) - 3\chi_\gamma y\,\mathrm{Int}\,K(2y)\right]S_\beta\hat{\boldsymbol{\beta}} \\ &+\left[\frac{\chi_\gamma}{\chi_e}S_b K_{1/3}(2y) - 3\chi_\gamma y K_{2/3}(2y)\right]S_e\hat{\mathbf{e}} \\ &+\left[\left(\frac{\chi_\gamma}{\chi_e}S_b^2 - 3\chi_e y\right)K_{1/3}(2y)\right. \\ &\left.-\,3\chi_\gamma y S_b K_{2/3}(2y)\right]\hat{\mathbf{b}}\Bigg\}\Bigg/\left[\left(2+3\chi_\gamma y\right)K_{2/3}(2y)\right. \\ &\left.-\,\mathrm{Int}\,K(2y) - \frac{\chi_\gamma}{\chi_e}S_b K_{1/3}(2y)\right].\end{aligned} \tag{2}$$

In addition, the polarization evolves under the combined effect of the classical spin precession following the T-BMT equation [27] and the no-photon-emission part of the radiation effect at all times [61], i.e.,

$$\begin{aligned}\frac{d\mathbf{S}}{dt} &= \boldsymbol{\Omega}\times\mathbf{S} + \frac{\alpha\left(\hat{\mathbf{b}} - S_b\mathbf{S}\right)}{\sqrt{3}\pi\tau_c\gamma\chi_e}\int_0^{\chi_e}\frac{\chi_\gamma}{\chi_e}K_{1/3}(2y)\,d\chi_\gamma, \\ \boldsymbol{\Omega} &= -\frac{e}{m_e c}\left[\left(a(\chi_e)+\frac{1}{\gamma}\right)\mathbf{B} - \frac{a(\chi_e)\gamma}{\gamma+1}(\boldsymbol{\beta}\cdot\mathbf{B})\,\boldsymbol{\beta}\right. \\ &\quad\left.-\left(a(\chi_e)+\frac{1}{\gamma+1}\right)\boldsymbol{\beta}\times\mathbf{E}\right],\end{aligned} \tag{3}$$

where $a(\chi_e) = (\alpha/\pi\chi_e)\int_0^\infty[u/(1+u)^3]L_{1/3}(2u/3\chi_e)\,du$ is the anomalous magnetic moment of the electron, taking the radiative correction into consideration [66], and $L_{1/3}(z) = \int_0^\infty \sin\left[(3z/2)\left(x + x^3/3\right)\right]dx$.

The simulation method is valid under the assumptions that $\gamma \gg 1$, $a_0 \gg 1$, and the electromagnetic fields are small with respect to the Schwinger limit field $E_{\rm crit} = m_e^2c^3/e\hbar \approx 1.32\times10^{18}$ V/m [43]. Our code is verified by reproducing the results of the Sokolov-Ternov effect and other spin-polarization models [20,67,68].

In the simulations, the initial electron beam possesses a width of 1 μm, a length of 5 μm, an angular divergence of 0.3 mrad, and an energy distribution centered around 5 GeV with a spread of 5%, while the circularly

polarized scattering laser beam possesses a wavelength of 800 nm, a Gaussian envelope with a waist radius of 5 μm, an intensity peaking at 2.14×10^{22} W/cm^2 ($a = a_0/\sqrt{2} = 100/\sqrt{2}$), and a hyperbolic secant temporal profile with a duration $\tau_{\mathrm{FWHM}} = 16$ fs. The collision angle is set to $\theta_{\mathrm{col}} = 3\pi/4$, and 10 million particles are simulated in total. The quantum efficiency parameter χ_e can be derived as $\chi_e \simeq \gamma(1 - \cos\theta_{\mathrm{col}})E_0/E_{\mathrm{crit}}$, and so the maximum χ_e is approximately 3.6.

III. RESULTS AND DISCUSSION

A. Filter settings

After the interaction, the electrons are scattered over a large angular range of tens of degrees and form an axisymmetric distribution with respect to the z axis (i.e., the original direction of the beam motion), as in the simulation results shown in Fig. 2. The larger the scattering angle, the smaller the number of electrons and the lower the electron energy. Most of the electrons are in the energy range of tens to hundreds of MeV and remain relativistic. For electrons in this energy range, when they are subjected to an electromagnetic field and change their motion direction, their spins are usually synchronously rotated. Thus we choose to set filters to obtain electrons with a high degree of transverse or longitudinal polarization in the direction we want, as shown in Fig. 1.

Considering that the scattering directions are distributed over a large angular range, to better understand the process of laser-electron interaction and describe the polarization for each electron, we utilize a modified frame (x', y', z') for each particle to analyze the spin polarization, as shown in Fig. 2(a). The modified frame (x', y', z') can be obtained by rotating the frame (x, y, z) through an angle θ around $\hat{\varphi}$, where θ is the angle between the motion direction $\hat{\boldsymbol{\beta}}$ and the z axis, and $\hat{\varphi} = \hat{z} \times \hat{\beta}$ is the rotation axis. The new frame (x', y', z') can be expressed in the laboratory frame as follows:

$$
\begin{aligned}
x' &= (\cos\theta + \varphi_x^2(1 - \cos\theta), \varphi_x\varphi_y(1 - \cos\theta), -\varphi_y \sin\theta), \\
y' &= (\varphi_x\varphi_y(1 - \cos\theta), \cos\theta + \varphi_y^2(1 - \cos\theta), \varphi_x \sin\theta), \\
z' &= (\varphi_y \sin\theta, -\varphi_x \sin\theta, \cos\theta) = \hat{\beta}. \qquad (4)
\end{aligned}
$$

By using the (x', y', z') frame, we can more easily define the transverse and longitudinal polarization for each electron and analyze the spin polarization process. $\hat{\mathbf{e}} = \mathbf{E}_{\mathrm{RF}}/|\mathbf{E}_{\mathrm{RF}}|$ and $\hat{\mathbf{b}} = \mathbf{B}_{\mathrm{RF}}/|\mathbf{B}_{\mathrm{RF}}|$ are in the (x', y') plane, and $\hat{\mathbf{e}} \times \hat{\mathbf{b}}$ is along the $-\hat{\boldsymbol{\beta}}$ axis. The average polarization calculated in the frame (x', y', z') can be considered as the result of detecting the polarization of electrons in different outgoing directions at infinite distance.

Through the polarization distribution, we can see that the polarization is mainly radial. The electrons with scattering angles above 0.17 rad mostly possess a radial polarization with a degree of around 80%, while the longitudinal and azimuthal polarizations are about 7% and 10%, respectively. However, the overall polarization of all scattered electrons is less than 3% for the longitudinal polarization and almost nil for the transverse polarization because of the axial symmetry of the polarization distribution.

Fortunately, the large angular distribution allows us to easily select polarized electrons with the same polarization direction and then obtain an electron beam with a high degree of overall polarization. Since the electron beam is collimated before the collision, the angular divergence and spatial size of the initial beam have little effect on the final distribution at such a large angular divergence of the scattering. When the electron beam travels some distance after the collision, the symmetry of the distribution is transferred to the spatial position of the scattered electrons, as shown in Figs. 1(b)–1(d). Then, we can set a filter for the required polarization direction to filter out electrons that possess a polarization in the opposite direction or a polarization with low degree, so as to obtain an electron beam with a high polarization in the required direction. For the transverse polarization, a rectangular filter can be employed to filter out the scattered electrons on one side, where the orientation of the filter is φ_{FT} and the cutoff scattering angle is θ_{FT}. Because of the axisymmetric nature of the scattering distribution, an overall polarization in other transverse directions can be easily obtained by rotating the filter around the z axis. For the longitudinal polarization, a circular filter can be employed to filter out electrons of lower polarization in the central area, where the cutoff scattering angle is θ_{FL}. The cutoff scattering angles for

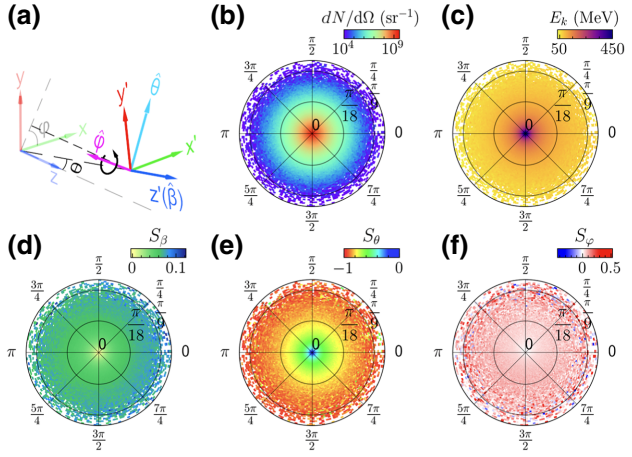

FIG. 2. (a) Relation between the coordinates and the vectors. (b) Number per solid angle $dN/d\Omega$, (c) kinetic energy E_k, (d) longitudinal polarization S_β, (e) radial polarization S_θ, and (f) azimuthal polarization S_φ versus the scattering direction of the electrons, where $S_\beta = \mathbf{S} \cdot \hat{\mathbf{p}}$, $S_\theta = (p_x S_y - p_y S_x)/p_\perp$, $S_\varphi = [p_z(p_x S_x + p_y S_y) - p_\perp^2 S_z]/(pp_\perp)$, $\hat{\mathbf{p}} = \mathbf{p}/|p|$, $p = |\mathbf{p}| = \sqrt{p_x^2 + p_y^2 + p_z^2}$, and $p_\perp = \sqrt{p_x^2 + p_y^2}$.

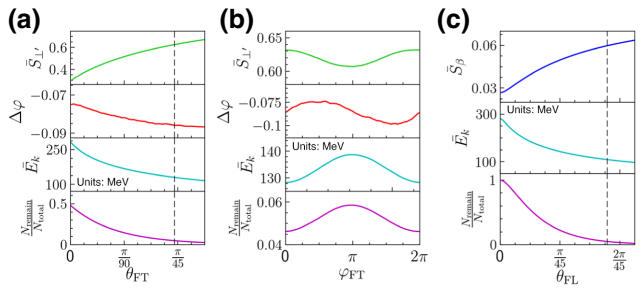

FIG. 3. Results for the filtered beam after applying (a) a filter for transverse polarization with $\varphi_{\rm FT} = 0$ and different values of $\theta_{\rm FT}$, (b) a filter for transverse polarization with $\theta_{\rm FT} = \pi/45$ and different values of $\varphi_{\rm FT}$, and (c) a filter for longitudinal polarization with different values of $\theta_{\rm FL}$. $\bar{S}'_{\perp}$ is the mean polarization component in the (x',y') plane, $\bar{E}_k$ is the mean kinetic energy of the filtered electron beam, and $\Delta\varphi$ is the angular difference between the direction of the overall transverse polarization $\mathbf{S}_{\perp'}$ and the filter orientation $\varphi_{\rm FT}$. The values corresponding to $N_{\rm remain}/N_{\rm total} = 5\%$ are marked with dashed lines.

both filters can be precisely controlled by sliding the filters along the z axis.

The results for the filtered beam with different cutoff scattering angles and filter orientations are shown in Fig. 3. The larger the cutoff scattering angle, the higher the overall polarization degree of the filtered beam, but at the same time the electron number is smaller and the average energy of the filtered beam is lower. For transverse polarization, about 62% polarization can be obtained with an electron-number ratio $N_{\rm remain}/N_{\rm total} = 5\%$. Under this condition, the cutoff scattering angle is about 0.07 rad, and the average energy is about 130 MeV. Because of the azimuthal polarization that emerges as a result of the effect of spin precession, the direction of the overall transverse polarization is not completely parallel to the filter direction $\varphi_{\rm FT}$, but has an angular difference of about 0.09 rad, which needs to be taken into account to obtain optimal results. Since the scattering laser beam and the electron beam do not collide head-on along the same axis, the results for different filter orientations are slightly different for the same cutoff scattering angle, but this does not affect our conclusions. For longitudinal polarization, a polarization degree of about 6% can be obtained with 5% of particles remaining, which is more than twice that in the case without filtering. In this case, the cutoff scattering angle is about 0.12 rad, and the average energy is about 108 MeV.

B. Theoretical analysis

The formation of the distribution can be explained by the motion of an electron in a plane electromagnetic wave. The electron is assumed to propagate along the z axis initially and to possess a momentum p_0, while the plane wave is assumed to propagate parallel to the x-z plane with a collision angle $\theta_{\rm col}$. The electron motion can easily be solved in the wave frame (x_L, y_L, z_L), where the wave propagates along the z_L axis. The frame (x_L, y_L, z_L) can be obtained by rotating the frame (x, y, z) around the y axis by $\theta_{\rm col}$. The wave can be represented by the normalized magnetic vector potential $\mathbf{a} = |e|\mathbf{A}/m_e c^2 = \delta a_0 \cos\phi\, \hat{\mathbf{x}}_L + \sqrt{1-\delta^2} a_0 \sin\phi\, \hat{\mathbf{y}}_L$, where $\phi = \omega_L t - \mathbf{k}\cdot\mathbf{r} + \phi_0$ is the phase of the wave, and δ is a polarization parameter such that $\delta = \pm 1/\sqrt{2}$ for a circularly polarized wave. Then, we can obtain expressions for the momenta in the frame (x_L, y_L, z_L) as [69]

$$\begin{aligned} p_{x_L} &= \mathbf{a}\cdot\hat{\mathbf{x}}_L - p_0 \sin\theta_{\rm col}, \\ p_{y_L} &= \mathbf{a}\cdot\hat{\mathbf{y}}_L, \\ p_{z_L} &= p_0\cos\theta_{\rm col} + \frac{\mathbf{a}^2 - 2p_0\sin\theta_{\rm col}\,\mathbf{a}\cdot\hat{\mathbf{x}}_L}{2(\gamma_0 - p_0\cos\theta_{\rm col})}, \end{aligned} \tag{5}$$

where $\gamma_0 = \sqrt{1+p_0^2}$ is the initial Lorentz factor of the electron. Note that here we use the dimensionless momentum (i.e., $p \to p/m_e c$) to simplify the expressions. For an initially ultrarelativistic electron (i.e., $\gamma_0 \gg 1$), we can make the approximation $\gamma_0 \approx p_0$ and utilize a coordinate transformation to obtain expressions in the frame (x, y, z), i.e.,

$$\begin{aligned} p_x &= -\delta a_0 \sin\phi' + \frac{a_0^2}{2\gamma_0 \tan(\theta_{\rm col}/2)}, \\ p_y &= \sqrt{1-\delta^2} a_0 \cos\phi', \\ p_z &= p_0 + \frac{a_0^2}{2\gamma_0(1/\cos\theta_{\rm col} - 1)} - \frac{\delta a_0}{\tan(\theta_{\rm col}/2)}\sin\phi', \end{aligned} \tag{6}$$

where $\phi' \approx (1-\cos\theta_{\rm col})\omega_L t + \phi'_0$.

To have an axisymmetric result, we require that

$$\begin{cases} \gamma_0 \gg a_0, \\ \theta_{\rm col} \in \left[\dfrac{\pi}{2}, \pi\right]. \end{cases} \tag{7}$$

When Eq. (7) is satisfied, the second term of p_x is far less than the amplitude of the periodic term, and so the motion in the x-y plane can be sketched as a circle for a circularly polarized wave, as shown in Fig. 4(a). The symmetry of the transverse motion of the electron results finally in an axisymmetric feature in the polarization. Since the electron circles synchronously with the wave, it can be calculated that the direction of the magnetic field in the rest frame, i.e., $\mathbf{B}_{\rm RF} = \gamma\,[\mathbf{B} - \boldsymbol{\beta}\times\mathbf{E} - (\gamma/(\gamma+1))\,(\boldsymbol{\beta}\cdot\mathbf{B})\,\boldsymbol{\beta}]$, is always close to the direction opposite to the transverse momentum (for $\delta = 1/\sqrt{2}$). According to Eq. (2), when the electron emits a high-energy photon, the electron is significantly polarized towards $-\hat{\mathbf{b}}$ and depolarized along the directions of $\hat{\boldsymbol{\beta}}$ and $\hat{\mathbf{e}}$. The higher the photon energy, the larger the polarization alteration. Thus, whenever an unpolarized electron

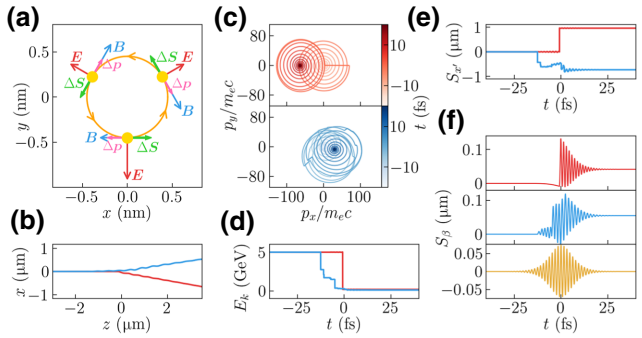

FIG. 4. (a) Illustrative diagram of electron motion and radiation. (b)–(f) Evolution of a hypothetical particle that emits only one high-energy photon during the interaction (red lines), a selected particle in the Monte Carlo simulation (blue lines), and a fully transversely polarized electron that is affected by spin precession but not by the effect of radiation (yellow line).

emits a high-energy photon, it obtains a high degree of polarization in the same direction as the current transverse momentum. On the other hand, the electron momentum undergoes a step alteration $\Delta\mathbf{p}$ in the direction opposite to the current momentum due to the radiation reaction. $\Delta\mathbf{p}$ is separate from the oscillating momentum, which changes the neutral direction and causes the electron to be scattered out of the original direction after the interaction. Therefore, if the electron emits only one photon in the whole interaction and this is a high-energy photon, as in the case of the hypothetical particle shown by red lines in Fig. 4, the electron eventually obtains a high degree of polarization towards $-\hat{\boldsymbol{\theta}}$. In the actual simulations, the electron always emits multiple photons during the interaction. However, for a short laser pulse, the ultimate state of the electron is mostly decided by the emission of a few of the highest-energy photons, as in the case of the simulated particle shown by blue lines in Fig. 4, and so the qualitative discussion above is still applicable.

As for the longitudinal polarization, generally, an electron cannot obtain growth in its longitudinal polarization from a rapidly changing periodic field such as a laser field in the sole presence of spin precession. The evolution of the longitudinal polarization due to the spin-precession effect can be written as [27]

$$\frac{dS_\beta}{dt} = -\frac{e}{m_e c}\mathbf{S}_\perp \cdot \left[a(\chi_e)\left(\hat{\boldsymbol{\beta}} \times \mathbf{B} + \beta\mathbf{E}\right) + \left(\beta - \frac{1}{\beta}\right)\mathbf{E}\right], \tag{8}$$

where $\mathbf{S}_\perp$ is the transverse component of $\mathbf{S}$. For the interaction between a relativistic electron and a circularly polarized laser field, when the polarization is mainly transverse (i.e., $S_\perp \gg S_\beta$), S_β can be approximately solved for as

$$S_\beta = \frac{S_\perp a(\chi_e) a_0}{\sqrt{2}} \cos\phi' + S_{\beta 0}, \tag{9}$$

where $S_{\beta 0}$ is the initial longitudinal polarization of the electron. It can be seen that the longitudinal polarization oscillates synchronously with the laser field and returns to its initial value $S_{\beta 0}$ when the electron leaves the laser field, as shown by the yellow line in Fig. 4(f). However, if the effect of radiation is taken into account, the results are different. When a high-energy photon is emitted, a polarization is generated in the direction of $-\hat{\mathbf{b}}$, and so we can calculate that $dS_\beta/dt \approx 0$ according to the relationship between the vector directions, which implies that the oscillation of S_β is at a peak or trough. In other words, the neutral position of the oscillation of the longitudinal polarization is altered after the emission. When the electron moves away from the laser pulse, the longitudinal polarization has increased compared with the beginning, as shown by the red line in Fig. 4(f). Because of symmetry, the neutral position moves towards the same direction whenever the emission occurs. Therefore, the effect accumulates for multiple emissions, as shown by the blue line in Fig. 4(f).

C. Influence of different initial conditions

In order to test the robustness of our scheme, we investigate the effect of different initial parameters, and the results for a filtered beam with 5% of the particles remaining are shown in Fig. 5. Except for the parameters in the figure, all initial parameters are the same as those mentioned in Sec. II. The electron has a high possibility of emitting photons with an energy comparable to that of the electron itself and thereby come close to the polarization limit once the quantum regime $\chi_e \sim 1$ is reached [61]. A further increase in χ_e does not make much difference in the polarization. Therefore, a transverse polarization with a degree above 60% is obtained for all laser intensities a_0 from 50 to 150. According to the analysis in Sec. III B,

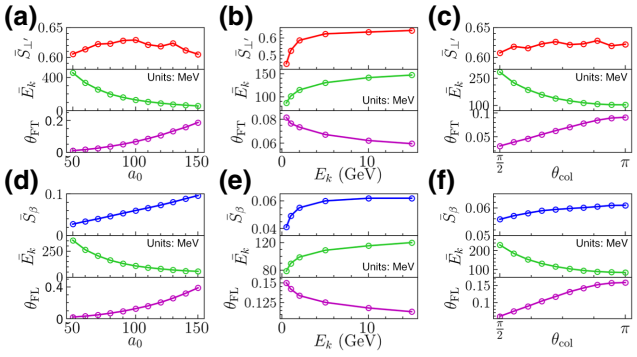

FIG. 5. Simulation results for the filtered beam with 5% of particles remaining for different values of the laser intensity a_0, initial beam energy E_k, and collision angle θ_{col}. (a)–(c) Filter for transverse polarization with $\varphi_{FT} = 0$. (d)–(f) Filter for longitudinal polarization.

the longitudinal polarization is transferred from the transverse polarization, and the final S_β is proportional to the laser intensity, which is also confirmed by our results. We obtain around 10% longitudinal polarization at $a_0 = 150$ (i.e., $I_0 = 6.42 \times 10^{22}$ W/cm^2, which can be achieved with current laser technologies). However, it should be noted that the larger the laser intensity, the stronger the radiation in the laser field, and the larger the radiation reaction force that the electron is subjected to. If the laser intensity is too large, the electrons will be scattered in every direction and lose almost all of their energy, which makes it impossible to utilize them as a beam. Therefore, it is impracticable to blindly increase the laser intensity to obtain a higher longitudinal polarization. As for the initial beam energy E_k, when the beam energy reaches about 5 GeV, a further increase in the initial energy does not lead to a significant increase in polarization, and this is also because the quantum regime $\chi_e \sim 1$ has been reached. An increase in the initial energy cannot greatly increase the energy of the final beam either, but this also implies that the method is efficient for a beam with a wide energy spread. Moreover, the average energy of the final beam is higher at a smaller collision angle $\theta_{\rm col}$, but the degree of polarization hardly decreases. Therefore, decreasing the collision angle may be a convenient way to increase the energy of the final beam, as long as the range of transverse motion of the electrons is smaller than the spatial size of the laser beam and the quantum regime $\chi_e \gtrsim 1$ is reached. From these simulation results, we can see that our scheme can be effectively applied for a variety of different initial parameters, thus demonstrating the robustness of our filtering method.

IV. CONCLUSIONS

In conclusion, we propose a filter mechanism for use with the collision of an initially unpolarized ultrarelativistic electron beam and an ultraintense circularly polarized laser pulse. After the collision, the polarization of the electrons is connected with their motion direction and spatial position, and thus we can filter out a part of the scattered electrons based on their spatial position to obtain a relativistic polarized electron beam with a high degree of polarization in a certain direction. The entire production process of relativistic polarized electron beams can be realized within tens of centimeters in our scheme, which makes the scheme much more compact compared with traditional methods based on large-scale accelerator devices. Moreover, polarization in various directions can be obtained in the same setup without the help of additional spin-rotation devices. Through numerical simulation utilizing a Monte Carlo code with consideration of spin developed by us, we obtain up to 62% polarization in any transverse direction and about 10% polarization in the longitudinal direction for the filtered beam with currently achievable laser intensities. We reveal the reason for the formation of the polarization distribution by analyzing the motion and spin evolution of relativistic electrons in a plane electromagnetic wave. Finally, the influence of different initial parameters on the results is investigated to demonstrate the robustness of our method. This method for producing relativistic polarized electron beams is practicable for experimental implementation and has potential applications in high-energy physics.

ACKNOWLEDGMENTS

The authors thank Z. Gong for helpful discussions. This work was supported by the NSFC (Grants No. 11921006 and No. 11535001) and the National Grand Instrument Project (Grant No. 2019YFF01014400). J.Y. was supported by the Natural Science Foundation of Hunan Province (Grant No. 12175058). The simulations were supported by the High-Performance Computing Platform at Peking University.

[1] E. Wigner, On unitary representations of the inhomogeneous Lorentz group, Ann. Math., 149 (1939).
[2] V. Bargmann, Irreducible unitary representations of the Lorentz group, Ann. Math., 568 (1947).
[3] V. Bargmann and E. P. Wigner, Group theoretical discussion of relativistic wave equations, Proc. Nat. Acad. Sci. **34**, 211 (1948).
[4] I. M. Shirokov, A group-theoretical consideration on the basis of relativistic quantum mechanics. I. The general properties of the inhomogeneous Lorentz group, J. Exp. Theor. Phys. **6**, 664 (1958).
[5] I. M. Shirokov, A group-theoretical consideration on the basis of relativistic quantum mechanics. II. Classification of the irreducible representations of the inhomogeneous Lorentz group, J. Exp. Theor. Phys. **6**, 919 (1958).
[6] I. M. Shirokov, A group-theoretical consideration on the basis of relativistic quantum mechanics. III. Irreducible representations of the classes p0 and o0, and the non-completely-reducible representations of the inhomogeneous Lorentz group, J. Exp. Theor. Phys. **6**, 929 (1958).
[7] I. M. Shirokov, Relativistic theory of polarization effects, J. Exp. Theor. Phys. **8**, 703 (1959).
[8] H. Tolhoek, Electron polarization, theory and experiment, Rev. Mod. Phys. **28**, 277 (1956).
[9] S. Mane, Y. M. Shatunov, and K. Yokoya, Spin-polarized charged particle beams in high-energy accelerators, Rep. Prog. Phys. **68**, 1997 (2005).
[10] P. Anthony, R. Arnold, H. Band, H. Borel, P. Bosted, V. Breton, G. Cates, T. Chupp, F. Dietrich, and J. Dunne, *et al.*, Determination of the Neutron Spin Structure Function, Phys. Rev. Lett. **71**, 959 (1993).
[11] K. Abe, T. Akagi, P. Anthony, R. Antonov, R. Arnold, T. Averett, H. Band, J. Bauer, H. Borel, and P. Bosted, *et al.*, Precision Measurement of the Deuteron Spin Structure Function g_1^d, Phys. Rev. Lett. **75**, 25 (1995).
[12] C. Y. Prescott, W. Atwood, R. Cottrell, H. Destaebler, E. L. Garwin, A. Gonidec, R. H. Miller, L. Rochester, T. Sato,

and D. Sherden, *et al.*, Parity Non-conservation in Inelastic Electron Scattering, Phys. Lett. B **77**, 347 (1978).
[13] P. Anthony, R. Arnold, C. Arroyo, K. Baird, K. Bega, J. Biesiada, P. Bosted, M. Breuer, R. Carr, and G. Cates, *et al.*, Observation of Parity Nonconservation in Møller Scattering, Phys. Rev. Lett. **92**, 181602 (2004).
[14] The Jefferson Lab Qweak Collaboration, Precision measurement of the weak charge of the proton, Nature **557**, 207 (2018).
[15] G. Moortgat-Pick, T. Abe, G. Alexander, B. Ananthanarayan, A. Babich, V. Bharadwaj, D. Barber, A. Bartl, A. Brachmann, and S. Chen, *et al.*, Polarized positrons and electrons at the linear collider, Phys. Rep. **460**, 131 (2008).
[16] H. Olsen and L. Maximon, Photon and electron polarization in high-energy bremsstrahlung and pair production with screening, Phys. Rev. **114**, 887 (1959).
[17] R. Märtin, G. Weber, R. Barday, Y. Fritzsche, U. Spillmann, W. Chen, R. DuBois, J. Enders, M. Hegewald, and S. Hess, *et al.*, Polarization Transfer of Bremsstrahlung Arising from Spin-Polarized Electrons, Phys. Rev. Lett. **108**, 264801 (2012).
[18] D. Abbott, P. Adderley, A. Adeyemi, P. Aguilera, M. Ali, H. Areti, M. Baylac, J. Benesch, G. Bosson, and B. Cade, *et al.*, Production of Highly Polarized Positrons using Polarized Electrons at MeV Energies, Phys. Rev. Lett. **116**, 214801 (2016).
[19] A. Sokolov and I. Ternov, Synchrotron radiation, Sov. Phys. J. **10**, 39 (1967).
[20] V. A. Bordovitsyn, *Synchrotron Radiation Theory and Its Development: In Memory of I M Ternov* (World Scientific, Singapore, 1999).
[21] C. Sun, J. Zhang, J. Li, W. Wu, S. Mikhailov, V. Popov, H. Xu, A. Chao, and Y. Wu, Polarization measurement of stored electron beam using Touschek lifetime, Nucl. Instrum. Methods Phys. Res. Sect. A: Accelerators, Spectrometers, Detectors and Associated Equipment **614**, 339 (2010).
[22] S. Mane, Y. M. Shatunov, and K. Yokoya, Siberian snakes in high-energy accelerators, J. Phys. G: Nucl. Part. Phys. **31**, R151 (2005).
[23] J. Buon and K. Steffen, Hera variable-energy "mini" spin rotator and head-on ep collision scheme with choice of electron helicity, Nucl. Instrum. Methods Phys. Res. Sect. A: Accelerators, Spectrometers, Detectors and Associated Equipment **245**, 248 (1986).
[24] D. T. Pierce, F. Meier, and P. Zürcher, Negative electron affinity GaAs: A new source of spin-polarized electrons, Appl. Phys. Lett. **26**, 670 (1975).
[25] D. T. Pierce and F. Meier, Photoemission of spin-polarized electrons from GaAs, Phys. Rev. B **13**, 5484 (1976).
[26] H. Batelaan, A. Green, B. Hitt, and T. J. Gay, Optically Pumped Electron Spin Filter, Phys. Rev. Lett. **82**, 4216 (1999).
[27] J. D. Jackson, *Classical Electrodynamics* (John Wiley & Sons, Hoboken, 1998), 3rd ed.
[28] B. Steiner, W. Ackermann, W. Muller, and T. Weiland, in *2007 IEEE Particle Accelerator Conference (PAC)* (IEEE, 2007), p. 170.
[29] N. F. Mott, The scattering of fast electrons by atomic nuclei, Proc. R. Soc. London Ser. A, Containing Papers Math. Phys. Charact. **124**, 425 (1929).
[30] T. J. Gay and F. Dunning, Mott electron polarimetry, Rev. Sci. Instrum. **63**, 1635 (1992).
[31] C. Møller, Zur Theorie des Durchgangs schneller Elektronen durch Materie, Ann. Phys. **406**, 531 (1932).
[32] P. Cooper, M. Alguard, R. Ehrlich, V. Hughes, H. Kobayakawa, J. Ladish, M. Lubell, N. Sasao, K. Schüler, and P. Souder, *et al.*, Polarized Electron-Electron Scattering at GeV Energies, Phys. Rev. Lett. **34**, 1589 (1975).
[33] M. Hauger, A. Honegger, J. Jourdan, G. Kubon, T. Petitjean, D. Rohe, I. Sick, G. Warren, H. Wöhrle, and J. Zhao, *et al.*, A high-precision polarimeter, Nucl. Instrum. Methods Phys. Res. Sect. A: Accelerators, Spectrometers, Detectors and Associated Equipment **462**, 382 (2001).
[34] D. Barber, H.-D. Bremer, M. Böge, R. Brinkmann, W. Brückner, C. Büscher, M. Chapman, K. Coulter, P. Delheij, and M. Düren, *et al.*, The HERA polarimeter and the first observation of electron spin polarization at HERA, Nucl. Instrum. Methods Phys. Res. Sect. A: Accelerators, Spectrometers, Detectors and Associated Equipment **329**, 79 (1993).
[35] M. Beckmann, A. Borissov, S. Brauksiepe, F. Burkart, H. Fischer, J. Franz, F. Heinsius, K. Königsmann, W. Lorenzon, and F. Menden, *et al.*, The longitudinal polarimeter at HERA, Nucl. Instrum. Methods Phys. Res. Sect. A: Accelerators, Spectrometers, Detectors and Associated Equipment **479**, 334 (2002).
[36] S. Belomesthnykh, A. Bondar, M. Yegorychev, V. Zhilitch, G. Kornyukhin, S. Nikitin, E. Saldin, A. Skrinsky, and G. Tumaikin, An observation of the spin dependence of synchrotron radiation intensity, Nucl. Instrum. Methods Phys. Res. Sect. A: Accelerators, Spectrometers, Detectors and Associated Equipment **227**, 173 (1984).
[37] C. N. Danson, C. Haefner, J. Bromage, T. Butcher, J.-C. F. Chanteloup, E. A. Chowdhury, A. Galvanauskas, L. A. Gizzi, J. Hein, and D. I. Hillier, *et al.*, Petawatt and exawatt class lasers worldwide, High Power Laser Sci. Eng. **7**, e54 (2019).
[38] J. W. Yoon, C. Jeon, J. Shin, S. K. Lee, H. W. Lee, I. W. Choi, H. T. Kim, J. H. Sung, and C. H. Nam, Achieving the laser intensity of 5.5×10^{22} W/cm^2 with a wavefront-corrected multi-PW laser, Opt. Express **27**, 20412 (2019).
[39] J. W. Yoon, Y. G. Kim, I. W. Choi, J. H. Sung, H. W. Lee, S. K. Lee, and C. H. Nam, Realization of laser intensity over 10^{23} W/cm^2, Optica **8**, 630 (2021).
[40] Z. Gong, Research progress on radiative spin polarized plasma, High Power Laser Part. Beams **35**, 012010 (2023).
[41] Y.-F. Li, R. Shaisultanov, K. Z. Hatsagortsyan, F. Wan, C. H. Keitel, and J.-X. Li, Ultrarelativistic Electron-Beam Polarization in Single-Shot Interaction with an Ultraintense Laser Pulse, Phys. Rev. Lett. **122**, 154801 (2019).
[42] H.-H. Song, W.-M. Wang, J.-X. Li, Y.-F. Li, and Y.-T. Li, Spin-polarization effects of an ultrarelativistic electron beam in an ultraintense two-color laser pulse, Phys. Rev. A **100**, 033407 (2019).
[43] D. Seipt, D. Del Sorbo, C. Ridgers, and A. Thomas, Theory of radiative electron polarization in strong laser fields, Phys. Rev. A **98**, 023417 (2018).
[44] D. Seipt, D. Del Sorbo, C. P. Ridgers, and A. G. Thomas, Ultrafast polarization of an electron beam in an intense bichromatic laser field, Phys. Rev. A **100**, 061402 (2019).

[45] T. Rakitzis, P. Samartzis, R. Toomes, T. Kitsopoulos, A. Brown, G. Balint-Kurti, O. Vasyutinskii, and J. Beswick, Spin-polarized hydrogen atoms from molecular photodissociation, Science **300**, 1936 (2003).

[46] T. P. Rakitzis, Pulsed-laser production and detection of spin-polarized hydrogen atoms, ChemPhysChem **5**, 1489 (2004).

[47] D. Sofikitis, L. Rubio-Lago, L. Bougas, A. J. Alexander, and T. P. Rakitzis, Laser detection of spin-polarized hydrogen from HCl and HBr photodissociation: Comparison of H- and halogen-atom polarizations, J. Chem. Phys. **129**, 144302 (2008).

[48] D. Sofikitis, C. S. Kannis, G. K. Boulogiannis, and T. P. Rakitzis, Ultrahigh-Density Spin-Polarized H and D Observed via Magnetization Quantum Beats, Phys. Rev. Lett. **121**, 083001 (2018).

[49] M. Wen, M. Tamburini, and C. H. Keitel, Polarized Laser-Wakefield-Accelerated Kiloampere Electron Beams, Phys. Rev. Lett. **122**, 214801 (2019).

[50] Y. Wu, L. Ji, X. Geng, Q. Yu, N. Wang, B. Feng, Z. Guo, W. Wang, C. Qin, and X. Yan, *et al.*, Polarized electron-beam acceleration driven by vortex laser pulses, New J. Phys. **21**, 073052 (2019).

[51] Y. Wu, L. Ji, X. Geng, Q. Yu, N. Wang, B. Feng, Z. Guo, W. Wang, C. Qin, and X. Yan, *et al.*, Polarized electron acceleration in beam-driven plasma wakefield based on density down-ramp injection, Phys. Rev. E **100**, 043202 (2019).

[52] Y. Wu, L. Ji, X. Geng, J. Thomas, M. Büscher, A. Pukhov, A. Hützen, L. Zhang, B. Shen, and R. Li, Spin Filter for Polarized Electron Acceleration in Plasma Wakefields, Phys. Rev. Appl. **13**, 044064 (2020).

[53] W. Leemans, A. Gonsalves, H.-S. Mao, K. Nakamura, C. Benedetti, C. Schroeder, C. Tóth, J. Daniels, D. Mittelberger, and S. Bulanov, *et al.*, Multi-GeV Electron Beams from Capillary-Discharge-Guided Subpetawatt Laser Pulses in the Self-Trapping Regime, Phys. Rev. Lett. **113**, 245002 (2014).

[54] A. Gonsalves, K. Nakamura, J. Daniels, C. Benedetti, C. Pieronek, T. De Raadt, S. Steinke, J. Bin, S. Bulanov, and J. Van Tilborg, *et al.*, Petawatt Laser Guiding and Electron Beam Acceleration to 8 GeV in a Laser-Heated Capillary Discharge Waveguide, Phys. Rev. Lett. **122**, 084801 (2019).

[55] I. Gol'dman, Intensity effects in Compton scattering, Sov. Phys. JETP **19**, 954 (1964).

[56] A. Nikishov and V. Ritus, Quantum processes in the field of a plane electromagnetic wave and in a constant field. I, Sov. Phys. JETP **19**, 529 (1964).

[57] V. Ritus, Quantum effects of the interaction of elementary particles with an intense electromagnetic field, J. Sov. Laser Res.;(United States) **6**, 497 (1985).

[58] Z. Gong, K. Z. Hatsagortsyan, and C. H. Keitel, Retrieving Transient Magnetic Fields of Ultrarelativistic Laser Plasma via Ejected Electron Polarization, Phys. Rev. Lett. **127**, 165002 (2021).

[59] Z. Gong, K. Z. Hatsagortsyan, and C. H. Keitel, Deciphering in situ electron dynamics of ultrarelativistic plasma via polarization pattern of emitted γ-photons, Phys. Rev. Res. **4**, L022024 (2022).

[60] Z. Gong, R. Hu, J. Yu, Y. Shou, A. Arefiev, and X. Yan, Radiation rebound and quantum splash in electron-laser collisions, Phys. Rev. Accel. Beams **22**, 093401 (2019).

[61] Y. Tang, Z. Gong, J. Yu, Y. Shou, and X. Yan, Radiative polarization dynamics of relativistic electrons in an intense electromagnetic field, Phys. Rev. A **103**, 042807 (2021).

[62] L. H. Thomas, The motion of the spinning electron, Nature **117**, 514 (1926).

[63] L. H. Thomas, I. The kinematics of an electron with an axis, London, Edinburgh, Dublin Philos. Mag. J. Sci. **3**, 1 (1927).

[64] V. Bargmann, L. Michel, and V. Telegdi, Precession of the Polarization of Particles Moving in a Homogeneous Electromagnetic Field, Phys. Rev. Lett. **2**, 435 (1959).

[65] R. Duclous, J. G. Kirk, and A. R. Bell, Monte Carlo calculations of pair production in high-intensity laser–plasma interactions, Plasma Phys. Controlled Fusion **53**, 015009 (2010).

[66] V. Baĭer, Radiative polarization of electrons in storage rings, Sov. Phys. Usp. **14**, 695 (1972).

[67] R.-T. Guo, Y. Wang, R. Shaisultanov, F. Wan, Z.-F. Xu, Y.-Y. Chen, K. Z. Hatsagortsyan, and J.-X. Li, Stochasticity in radiative polarization of ultrarelativistic electrons in an ultrastrong laser pulse, Phys. Rev. Res. **2**, 033483 (2020).

[68] Y.-F. Li, Y.-Y. Chen, W.-M. Wang, and H.-S. Hu, Production of Highly Polarized Positron Beams via Helicity Transfer from Polarized Electrons in a Strong Laser Field, Phys. Rev. Lett. **125**, 044802 (2020).

[69] P. Gibbon, *Short Pulse Laser Interactions with Matter* (Imperial College Press, London, 2005).